

Thermal Transport Along the Dislocation Line in Silicon Carbide

Yuxiang Ni,¹ Shiyun Xiong,² Sebastian Volz,² and Traian Dumitrică^{1,*}

¹Department of Mechanical Engineering, University of Minnesota, 111 Church Street SE, Minneapolis, Minnesota 55455, USA

²Laboratoire d'Énergétique Moléculaire et Macroscopique, CNRS UPR 288, Ecole Centrale Paris,

Grande Voie des Vignes, 92295 Châtenay-Malabry, France

(Received 12 June 2014; published 18 September 2014)

We elucidate thermal conductivity along the screw dislocation line, which represents a transport direction inaccessible to classical theories. By using equilibrium molecular dynamics simulations, we uncover a Burgers vector dependent thermal conductivity reduction in silicon carbide. The effect is uncorrelated with the classical modeling and originates in the highly deformed core region, which represents a significant source of anharmonic phonon-phonon scattering. High strain reduces the phonon relaxation time, especially in the longitudinal acoustic branches, and creates an effective internal thermal resistance around the dislocation axis. Our results have implications for designing materials useful for high-temperature electronics and thermoelectric applications.

DOI: 10.1103/PhysRevLett.113.124301

PACS numbers: 44.10.+i, 63.20.-e, 65.80.-g

The atomic-scale dislocation [1] defects are essential in determining the physical properties of crystalline materials, including the thermal properties [2–4]. Dislocation-induced deviations from the perfect lattice give rise to various phonon scattering processes. Klemens [5] has captured the linear-elastic strain field of a screw dislocation (SD) using a second-order perturbation treatment. He disregarded the Burgers vector dependent distortion in the SD core region and approximated it as a line of vacancy defects [4], which can also be treated perturbatively. This early model focused on the phonon scattering *perpendicular* onto the dislocation line, and can be summarized by the phonon relaxation time relations $1/\tau_s \propto b^2\omega$ and $1/\tau_c \propto \omega^3$. Here τ_s and τ_c are the linear elastic and dislocation core phonon relaxation times, b is the magnitude of the Burgers vector, and ω the phonon frequency. In spite of its well-recognized quantitative discrepancies [2,4], the classical model [5] is still used nowadays. It correctly predicts the experimentally observed reduction in thermal conductivity, including the temperature (T) T^2 dependence. Different scattering directions have also been considered to account for the random orientation of dislocations in a crystal. For example, Ohashi [6] proposed that $1/\tau_s$ is, in addition, proportional to $\sin^2\varphi$, where φ is the angle of incidence of the phonons with the dislocation line.

The dislocation-thermal transport interaction *along* the SD line case is not accounted for by the classical theory [5]. This limiting case is important not only for completing our fundamental understanding, but also for predicting thermal transport in the recently discovered class of nanomaterials synthesized by engaging SDs [7–11]. Examples of such nanomaterials include the vertical nanowire (NW) arrays whose growth has been driven by SDs in the underlying substrates [10] and where each individual NW stores a SD oriented along the long NW axis. In this Letter, we examine thermal transport along the SD axis from the microscopical

perspective of the unevenly distributed strain in and around the highly deformed core region. We are focusing on silicon carbide (SiC), a wide band-gap semiconductor material in which SDs are long established [12,13]. Because of the inability of analytical theories to capture accurately the core region of a SD with specific Burgers vectors, we make recourse to atomistic molecular dynamics (MD) simulations and the Green-Kubo [14] method [15,16]. Interestingly, the linear elastic strain field of the SD, which exhibits radial symmetry and contains no tensile or compressive components, suggests that this limiting case is not worth considering. This is because no phonons scattering occurs ($1/\tau_s = 0$) when $\varphi = 0$. Contrary to the conventional wisdom, we uncover a Burgers vector dependent thermal conductivity decrease along the SD line direction. The underlying mechanism is clearly explained after a thorough comparison of the SD and pristine SiC structures in terms of phonon relaxation times, phonon group velocities, vibrational density of states, and internal thermal resistance distributions.

Our large-scale MD simulations, performed with LAMMPS [17], considered a set of screw dislocated and pristine β -SiC $\langle 110 \rangle$ NWs with square cross-sectional areas ranging from 4×4 nm to 7×7 nm. The periodic boundary condition (PBC) was applied only in the z direction on supercells 7 nm in length. This length value was selected after a preliminary study [18] of finite-size effects [16], which determined thermal conductivity convergence for 7 nm or longer supercells. SDs were introduced to the pristine structures with the axis (along the z direction) located at the center; see Fig. 1. We considered a minimal Burgers vector of magnitude $1b$ and $2b$, where $b = 3.08$ Å. In the $1b$ case the core structure is morphologically equivalent with the Hornstra core structure of silicon [19]. Note that the NW system has the advantage of not requiring the need to consider multiple dislocations in each

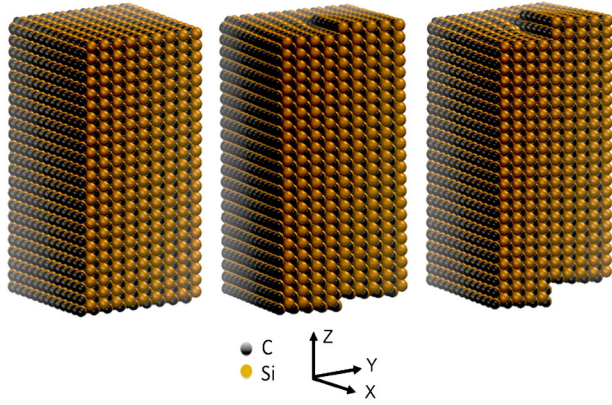


FIG. 1 (color online). Supercells for the SiC calculations: pristine (left), $1b$ (center), and $2b$ (right) screw dislocated. The heat carrying direction is z . The cross-section dimensions are 4×4 nm. Length is 7 nm.

unit cell, as it is done under full PBCs [20]. A possible complication is the Eshelby twist introduced by the SD [7–11,21–23], which removes the translational symmetry of the pristine NW structure. Nevertheless, our previous nonequilibrium MD calculations demonstrated that this effect is unimportant for thermal transport [19] and therefore will not be accounted for here. The interatomic Si-C interactions were described with a Tersoff-type potential and the parameters proposed by Porter *et al.* [24]. This microscopic model is sufficiently robust for predicting the experimentally observed acoustic phonon spectrum [25] and the thermal conductivity of SiC bulk [25].

In preparation for the thermal conductivity calculations, the initial structures were relaxed using a conjugate gradient energy minimization algorithm. After the relaxation, all atoms in the dislocation core remain fourfold coordinated and no homoelemental (Si-Si and C-C) bonds were created. Nevertheless, the Si-C bonds undergo large deformations. For example, in our atomistically computed structures we identified bonds 1.94 Å in length that are located in the core of the $2b$ NW. (The centrally located bonds in the pristine NW measure 1.88 Å.) The NW structures were evolved for 200 ps in the canonical ensemble in order to impose a 300 K temperature, and next in the microcanonical ensemble for another 200 ps in order to achieve thermal equilibrium. The MD time step was set to 0.25 fs. Finally, MD runs with lengths equal to 600 ps were carried out to take the thermal conductivity along the z -axis (κ_z) measurement. κ_z was computed based on the instantaneous z component of the microscopic heat flux

$$j_z(t) = \frac{1}{V} \left[\sum_{i,j,j \neq i} \frac{1}{2} z_{ij} \cdot (\mathbf{F}_{ij} \cdot \mathbf{v}_i) + \frac{1}{6} \sum_{i,j,k,k \neq i \neq j} (z_{ij} + z_{ik}) \cdot (\mathbf{F}_{ijk} \cdot \mathbf{v}_i) \right], \quad (1)$$

and the Green-Kubo formula

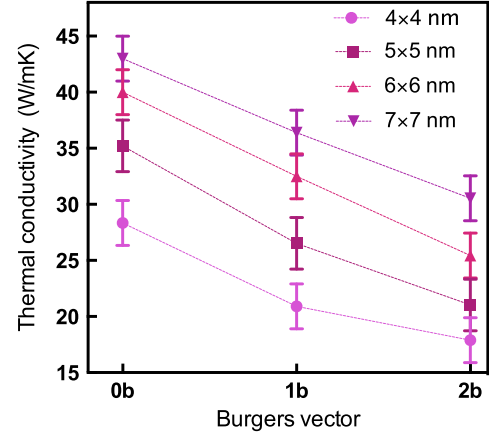


FIG. 2 (color online). Thermal conductivity along screw dislocation line in SiC NWs with different cross-sectional areas, as a function of the magnitude of Burgers vector. $0b$ is the pristine NW. The error bars quantify the statistical errors in the simulations.

$$\kappa_z = \frac{V}{k_B T^2} \int_0^{+\infty} \langle j_z(t) j_z(0) \rangle dt. \quad (2)$$

In these expressions, z_{ij} is the z component of the interatomic distance vector, \mathbf{v} is the atomic velocity, and \mathbf{F} the interatomic force. z_{ij} , \mathbf{v} , and \mathbf{F} are t dependent. k_B is the Boltzmann constant and V the system volume. The angular brackets denote the ensemble average, performed here over the microstates of twenty independent MD measurement runs. We note that Eq. (1) indicates that j_z could be still influenced by the strain field of the SD due to the vectorial nature of \mathbf{v} and \mathbf{F} .

Our main result is summarized in Fig. 2, which displays an important reduction in κ_z with increasing b . As expected, κ_z is also reduced as the cross-sectional area decreases. The later effect is related to the coupling of the characteristic dimensions of the NW with the phonon mean free path and involves phonon-boundary scattering and the phonon confinement process [26]. Nevertheless, the decrease of κ_z with b occurs regardless of the cross-sectional dimensions, and should occur to the same extent in bulk. It is useful to note that throughout the MD runs, the crystalline β -SiC arrangement was preserved. The dislocation line stayed at the center during the MD runs, indicating that another well-recognized conductivity reduction mechanism, by dislocation motion [5], is not present in our data.

It is very useful to analyze the observed hindering of the phonon transport using the concept of phonon relaxation time (τ_z). τ_z , which is assigned to each phonon mode, represents a measure of the average time between successive phonon scattering events. In Fig. 3(a), τ_z was computed directly from the equilibrium MD runs by using the spectral energy density analysis approach [18,27,28]. Acoustic phonons play a central role in thermal conduction

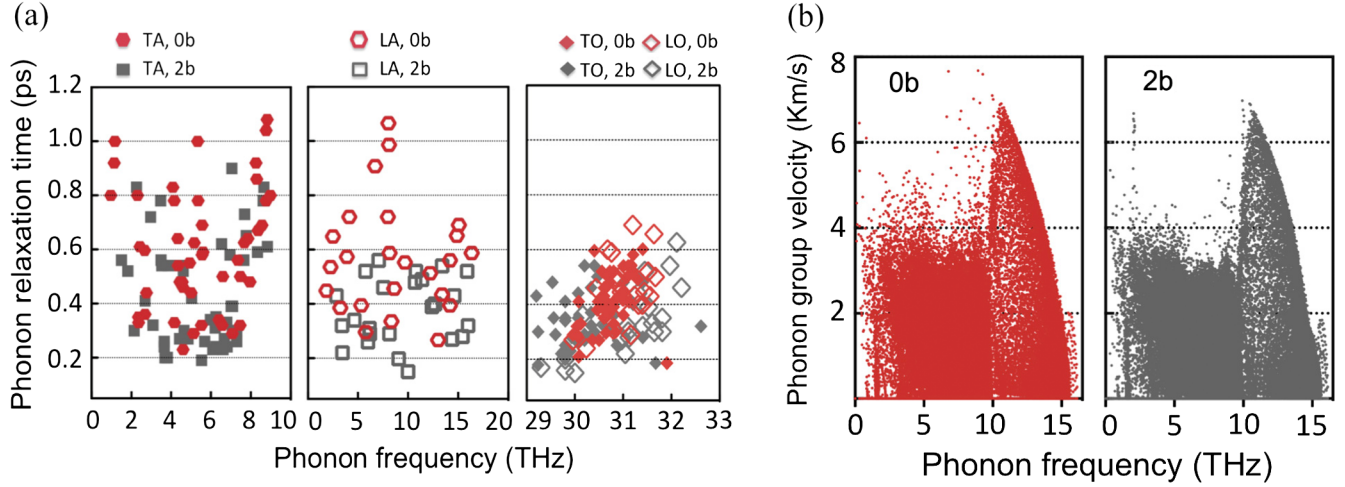


FIG. 3 (color online). (a) Comparison of τ_z in pristine and SD NW with $2b$: transverse acoustic (left), longitudinal acoustic (middle), and transverse and longitudinal optical (right) modes. (b) Comparison of acoustic phonon group velocities in pristine (left) and SD NW (right) with $2b$. The NW cross-sectional dimensions are 6×6 nm.

as in general they have longer τ_z than the optical ones. The presence of SD leads to a significant reduction of τ_z over the full frequency range. For an overall picture, we compare in Table I the average values of τ_z computed for the different phonon branches. We observe a particularly large $\bar{\tau}_z$ reduction by 36.2% for the heat carrying LA modes, which is consistent with the percentage reduction in κ_z shown in Fig. 2. This observation correlates well with the comparison shown in Fig. 3(b) of the group velocity (v_z^g) along z , which is another key contributor to κ_z . v_z^g for each phonon mode was computed based on lattice dynamics [18,29]. While a slight $v_{g,z}$ decrease could be observed in the SD case, the main values and its distribution over frequency remained unaltered. Thus, scattering is predominant over group velocity in κ_z reduction.

The lattice distortion in the core region impacts the phonon modes. For more insight into this effect, we have computed the vibrational density of states (VDOS). We decomposed in Fourier space the time correlation function of the atomic velocities of the atoms located inside a cylinder with a radius equal to b and an axis coinciding with the dislocation axis. Figure 4 shows the VDOS of the pristine and SD. Differences appear in the optical phonon range (> 29 THz). Moreover, additional peaks emerge in the high frequency range (37–55 THz). These new frequencies can be ascribed to the severe lattice distortion at the core. Nevertheless, what is important here is the

TABLE I. Comparison of the average of τ_z , $\bar{\tau}_z$ on various phonon branches in pristine and SD NW with $2b$.

Burgers vector	Phonon branch:	TA	LA	TO	LO
0	$\bar{\tau}_z$ (ps):	0.60	0.58	0.41	0.45
$2b$	$\bar{\tau}_z$ (ps):	0.44	0.37	0.32	0.33

observation that VDOS practically coincide over the important acoustic phonon range (0–17 THz). Thus, differences in structures cannot explain the κ_z reduction.

We relate the origin of κ_z reduction to the enhanced anharmonicity created by the SD dislocation strain field, especially the nonlinear elastic field located at the core. We support this explanation with the computed internal thermal resistance distributions along the x and y directions shown in Fig. 5. R_x and R_y , the thermal resistances between adjacent y - z and x - z atomic planes, respectively, were computed from equilibrium MD with the method of Rajabpour and Volz [18,30]. Away from the NW edge and core, the thermal resistance values of 1.2 - 1.5×10^{-10} m² K/W agree well with what was obtained in previous investigations of similar systems [26]. R_x and R_y are increasing at the NW faces. The resistances at the faces are comparable for both pristine and SD NW

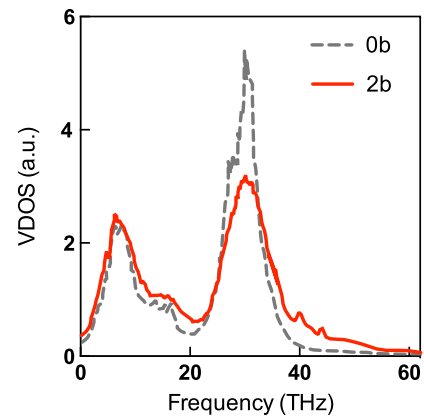


FIG. 4 (color online). Phonon density of states of pristine SiC NW (dashed line) and SD NW with $2b$ Burgers vector (solid line).

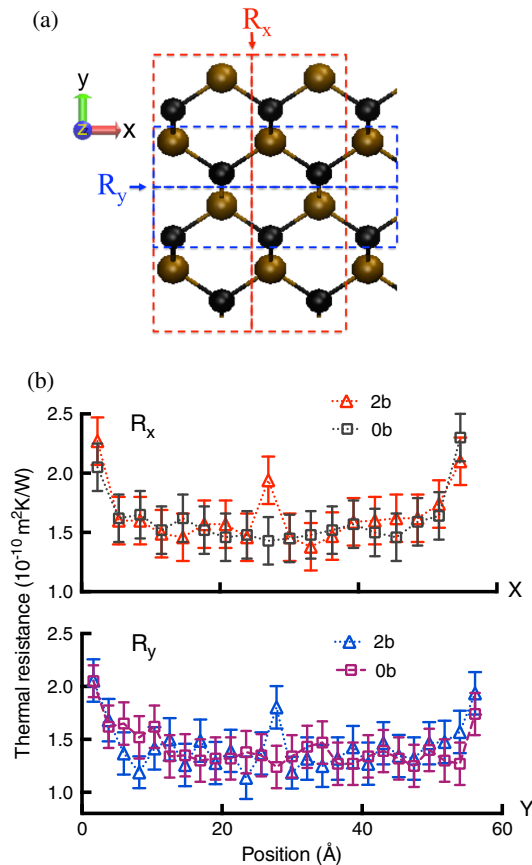


FIG. 5 (color online). (a) Schematics for the definition of the internal thermal resistance between adjacent atomic layers (enclosed with dashed squares) along the x - z and y - z planes. (b) Internal thermal resistance along x (upper) and along y (lower): a comparison between pristine and $2b$ SD NW. On the horizontal axis, the position is measured from a NW face. The NW cross-sectional dimensions are 6×6 nm.

configurations. Phonons propagating along the NW axis may still have a wave vector component perpendicular of the NW surface. These phonons, having incident angles $\varphi \neq 0$, will scatter in the same manner onto the surfaces of pristine and SD NWs. The thermal resistances between the two structures differ significantly only at the NW center. This comparison shows that the differences in κ_z reported in Fig. 2 are due to the dislocation core and not due to potential differences in surface scattering. Judging from the values of thermal resistances at the NW center, we infer that the core region of the SD resists heat flow at a level comparable with the NW surfaces. Thus, the SD core is an important source of scattering for phonons with $\varphi \neq 0$ that are propagating along the z axis. We emphasize that the underlying mechanism originates in the b -dependent severe distortion of the core bonds causing an increased anharmonic phonon-phonon scattering (umklapp scattering). This mechanism is different from and uncorrelated with one in the classical model utilized by Klemens [5], where

the dislocation core is emulated by a line of vacancies. In the Klemens model, thermal conductivity reduction involves thermal mechanisms involving missing mass and missing linkages, which are both associated with the line of vacancies.

In conclusion, direct MD simulations enabled us to replace the usual line of vacancy defects classical approximation of the SD core region with a realistic structural microscopic representation. We uncover an unexpected thermal conductivity reduction along the SD line of SiC. The effect originates in the enhanced phonon-phonon scattering caused by the anharmonicity in the highly distorted core region. As high strain is intrinsic to dislocations, the mechanism should be transferable to other materials and nanostructures. Our b dependent thermal conductivity modulation prediction can be investigated with modern experimental techniques, that could focus either on individual NWs, such as by employing micro-devices [31], or on NW arrays, such as time-domain thermoreflectance [32]. In view of the current efforts on controlled SD growth of nanomaterials [7–11], the b dependent thermal transport along the dislocation line presents particular importance. It could be exploited for designing advanced materials for applications which demand extremizing (maximizing or minimizing) thermal transport. Wide-band gap semiconductor materials, such as SiC, are of interest for high temperature electronics. Dislocations with lower b vectors are desirable in order to minimize heat dissipation. On the contrary, for thermoelectric application, dislocations with larger b are desirable in order to scatter phonons. In combination with various other structural effects [33–35], SD can reduce lattice thermal conductivity and boost thermoelectric performance.

Y. N. and T. D. acknowledge partial funding from NSF CMMI Grants No. 1332228 and No. 1333158. Computations were performed at the Minnesota Supercomputing Institute.

*Corresponding author.
dtraian@umn.edu

- [1] G. I. Taylor, *Proc. R. Soc. A* **145**, 362 (1934).
- [2] R. L. Sproull, M. Moss, and H. Weinstock, *J. Appl. Phys.* **30**, 334 (1959).
- [3] H. Bross, A. Seeger, and R. Haberkorn, *Phys. Status Solidi (b)* **3**, 1126 (1963).
- [4] P. Carruthers, *Rev. Mod. Phys.* **33**, 92 (1961).
- [5] P. G. Klemens, *Solid State Phys.* **7**, 1 (1958).
- [6] K. Ohashi, *J. Phys. Soc. Jpn.* **24**, 437 (1968).
- [7] M. J. Bierman, Y. K. A. Lau, A. V. Kvit, A. L. Schmitt, and S. Jin, *Science* **320**, 1060 (2008).
- [8] B. W. Jacobs, M. A. Crimp, K. McElroy, and V. M. Ayres, *Nano Lett.* **8**, 4353 (2008).
- [9] J. Zhu, H. Peng, A. F. Marshall, D. M. Barnett, W. D. Nix, and Y. Cui, *Nat. Nanotechnol.* **3**, 477 (2008).
- [10] S. A. Morin and S. Jin, *Nano Lett.* **10**, 3459 (2010).

- [11] F. Meng, S. A. Morin, A. Forticaux, and S. Jin, *Acc. Chem. Res.* **46**, 1616 (2013).
- [12] S. Amelinckx, *Nature (London)* **167**, 939 (1951).
- [13] V. R. Verma, *Nature (London)* **167**, 939 (1951).
- [14] R. Kubo, M. Toda, and N. Hashitsume, *Statistical Physics II* (Springer, Berlin, 1985).
- [15] For a review of this method see S. P. A. Gill, in *Trends in Computational Nanomechanics: Transcending Length and Time Scales*, edited by T. Dumitrică (Springer, Netherlands, 2010).
- [16] K. V. Tretyakov and S. Scandolo, *J. Chem. Phys.* **120**, 3765 (2004).
- [17] S. Plimpton, *J. Comput. Phys.* **117**, 1 (1995).
- [18] See Supplemental Material at <http://link.aps.org/supplemental/10.1103/PhysRevLett.113.124301> for more information on finite size effects, phonon relaxation time, group velocity, and thermal resistance calculations.
- [19] S. Xiong, J. Ma, S. Volz, and T. Dumitrică, *Small* **10**, 1756 (2014).
- [20] J. R. K. Bigger, D. A. McInnes, A. P. Sutton, M. C. Payne, I. Stich, R. D. King-Smith, D. M. Bird, and L. J. Clarke, *Phys. Rev. Lett.* **69**, 2224 (1992).
- [21] I. Nikiforov, D.-B. Zhang, and T. Dumitrică, *J. Phys. Chem. Lett.* **2**, 2544 (2011).
- [22] E. Akatyeva and T. Dumitrică, *Phys. Rev. Lett.* **109**, 035501 (2012).
- [23] E. Akatyeva, L. Kou, I. Nikiforov, Th. Frauenheim, and T. Dumitrică, *ACS Nano* **6**, 10042 (2012).
- [24] L. J. Porter, J. Li, and S. Yip, *J. Nucl. Mater.* **246**, 53 (1997).
- [25] J. Li, L. J. Porter, and S. Yip, *J. Nucl. Mater.* **255**, 139 (1998).
- [26] K. Termentzidis, T. Barreateau, Y. Ni, S. Merabia, X. Zianni, Y. Chalopin, Y. P. Chantrenne, and S. Volz, *Phys. Rev. B* **87**, 125410 (2013).
- [27] J. A. Thomas, J. E. Turney, R. M. Iutzi, C. H. Amon, and A. J. H. McGaughey, *Phys. Rev. B* **81**, 081411 (2010).
- [28] B. Qiu, H. Bao, G. Zhang, Y. Wu, and X. Ruan, *Comput. Mater. Sci.* **53**, 278 (2012).
- [29] H. Zhao and J. B. Freund, *J. Appl. Phys.* **97**, 024903 (2005).
- [30] A. Rajabpour and S. Volz, *J. Appl. Phys.* **108**, 094324 (2010).
- [31] F. Zhou, J. Szczech, M. T. Pettes, A. L. Moore, S. Jin, and L. Shi, *Nano Lett.* **7**, 1649 (2007).
- [32] X. Wang, C. D. Liman, N. D. Treat, M. L. Chabinyc, and D. G. Cahill, *Phys. Rev. B* **88**, 075310 (2013).
- [33] P. Martin, Z. Aksamija, E. Pop, and U. Ravaioli, *Phys. Rev. Lett.* **102**, 125503 (2009).
- [34] F. Sansoz, *Nano Lett.* **11**, 5378 (2011).
- [35] J. Carrete, L. J. Gallego, L. M. Varela, and N. Mingo, *Phys. Rev. B* **84**, 075403 (2011).